Systems/Circuits

Induction of Activity-Dependent Plasticity at Auditory Nerve Synapses

Nicole F. Wong and Matthew A. Xu-Friedman
Department of Biological Sciences, University at Buffalo, State University of New York, Buffalo, New York 14260

Exposure to nontraumatic noise *in vivo* drives long-lasting changes in auditory nerve synapses, which may influence hearing, but the induction mechanisms are not known. We mimicked activity in acute slices of the cochlear nucleus from mice of both sexes by treating them with high potassium, after which voltage-clamp recordings from bushy cells indicated that auditory nerve synapses had reduced EPSC amplitude, quantal size, and vesicle release probability (P_r). The effects of high potassium were prevented by blockers of nitric oxide (NO) synthase and protein kinase A. Treatment with the NO donor, PAPA-NONOate, also decreased P_r, suggesting NO plays a central role in inducing synaptic changes. To identify the source of NO, we activated auditory nerve fibers specifically using optogenetics. Strobing for 2 h led to decreased EPSC amplitude and P_r, which was prevented by antagonists against ionotropic glutamate receptors and NO synthase. This suggests that the activation of AMPA and NMDA receptors in postsynaptic targets of auditory nerve fibers drives release of NO, which acts retrogradely to cause long-term changes in synaptic function in auditory nerve synapses. This may provide insight into preventing or treating disorders caused by noise exposure.

Key words: **auditory nerve; bushy cell; cochlear nucleus; endbulb of Held; long-term depression; synaptic plasticity**

Significance Statement

Auditory nerve fibers undergo long-lasting changes in synaptic properties in response to noise exposure *in vivo*, which may contribute to changes in hearing. Here, we investigated the cellular mechanisms underlying induction of synaptic changes using high potassium and optogenetic stimulation *in vitro* and identified important signaling pathways using pharmacology. Our results suggest that auditory nerve activity drives postsynaptic depolarization through AMPA and NMDA receptors, leading to the release of nitric oxide, which acts retrogradely to regulate presynaptic neurotransmitter release. These experiments revealed that auditory nerve synapses are unexpectedly sensitive to activity and can show dramatic, long-lasting changes in a few hours that could affect hearing.

Introduction

Changes in neurons and synapses of the central auditory system are thought to underlie a number of auditory disorders, including tinnitus and language processing disorders (Whitton and Polley, 2011; Shore and Wu, 2019). Low-intensity, nontraumatic noise exposure can lead to changes in acoustic responses in the central auditory system, including in the cochlear nucleus, inferior colliculus, and auditory cortex (Pienkowski and Eggermont, 2009; Munguia et al., 2013; Pienkowski et al., 2013; Lau et al., 2015; Sheppard et al., 2017). Extensive work in nonauditory systems has revealed diverse mechanisms by which activity can drive long-lasting changes in synapses (Turrigiano, 2008; Castillo, 2012). These processes can involve activation of postsynaptic NMDA or metabotropic glutamate receptors that cause changes in postsynaptic receptor expression (Malenka and Bear, 2004) or presynaptic changes in the probability of vesicle release (P_r; Branco and Staras, 2009; Vitureira et al., 2012) through retrograde signaling by endocannabinoids or nitric oxide (NO; Regehr et al., 2009). Some of these signaling pathways have been implicated in stages of the auditory pathway, including in the dorsal cochlear nucleus, medial nucleus of the trapezoid body, and superior paraolivary nucleus (Tzounopoulos et al., 2004; Steinert et al., 2008; Yassin et al., 2014; Kopp-Scheinpflug and Forsythe, 2021).

Recently, it has become clear that acoustic activity *in vivo* can cause long-lasting changes at auditory nerve synapses in the anteroventral cochlear nucleus (AVCN). These synapses, called endbulbs of Held, are made onto bushy cells (BCs; Lorente de Nó, 1981; Ryugo and Fekete, 1982; Ryugo and Sento, 1991).

Received Apr. 5, 2022; revised May 26, 2022; accepted June 25, 2022.

Author contributions: M.A.X.-F. and N.F.W. designed research; N.F.W. performed research; M.A.X.-F. and N.F.W. analyzed data; M.A.X.-F. and N.F.W. wrote the paper.

This work was supported by the National Institute on Deafness and Other Communication Disorders (Grant RO1 DC015508). We thank J. Chow, C. Cook, J. Engel, V. Gellatly, T. Ngodup, G. Si, and X. Zhuang for help throughout this project; A. Zimmer, who donated the CB1R KO mice; and C. Weisz, who provided the Math5-Cre mice.

The authors declare no competing financial interests.

Correspondence should be addressed to Matthew A. Xu-Friedman at mx@buffalo.edu.

https://doi.org/10.1523/JNEUROSCI.0666-22.2022

Exposure to moderate, nontraumatic levels of noise leads to decreased P_r in endbulbs and increased number of releasable vesicles (N; Ngodup et al., 2015), whereas conductive hearing loss leads to increased P_r and decreased N (Zhuang et al., 2017). Because these changes occur at the very start of the auditory pathway, they could have a major impact on all downstream processing, including sound localization, in which BCs play a central role (Grothe et al., 2010; Kuenzel, 2019). It is therefore important to identify the signaling pathways driving synaptic changes.

Here, we developed approaches to induce changes at auditory nerve synapses in acute slices by treating them with high potassium or strobing with optogenetics. These techniques triggered plasticity in a few hours, which indicates an unexpected level of flexibility for a synapse that has long been considered a simple relay. Our experiments revealed that induction depended on postsynaptic glutamate receptor activation and retrograde signaling by NO. These experiments provide new insight into how auditory nerve synapses are affected by acoustic activity, which may lead to better understanding of how synaptic dysfunction could arise with auditory disorders.

Materials and Methods

All experiments were performed with the approval of the University at Buffalo Institutional Animal Care and Use Committee. Electrophysiology experiments used CBA/CaJ mice (stock #654, The Jackson Laboratory) and CB1R KO mice (a gift from Andreas Zimmer; Zimmer et al., 1999) of either sex ranging in age from postnatal day (P)16 to P28. The CB1R KO mice (see Fig. 4) were backcrossed into the CBA/CaJ line for over 10 generations. Experiments (see Fig. 2) also used offspring from mice expressing ChR2-EYFP (originally Ai32 mice, stock #024109, The Jackson Laboratory, back-crossed into the CBA/CaJ line for over 10 generations) crossed with Math5-Cre mice (Yang et al., 2003; Kronander et al., 2017; backcrossed into the CBA/CaJ line for four generations). We refer to the offspring as Math5-EYFP mice.

Electrophysiology. To prepare brain slices, mice were anesthetized with ketamine/xylazine (200:10 mg/kg) and perfused transcardially with ice-cold sucrose solution containing the following (in mM): 76 NaCl, 75 sucrose, 25 $NaHCO_3$, 25 glucose, 2.5 KCl, 1.25 NaH_2PO_4, 7 $MgCl_2$, and 0.5 $CaCl_2$. The brain was removed, and sagittal slices were cut using a Campden Integraslice 7550 MM or a Leica VT1200 (142 µm) and incubated in standard recording solution containing the following (in mM): 125 NaCl, 26 $NaHCO_3$, 20 glucose, 2.5 KCl, 1.25 NaH_2PO_4, 1 $MgCl_2$, 1.5 $CaCl_2$, 4 Na L-lactate, 2 Na-pyruvate, and 0.4 Na L-ascorbate, bubbled with 95% O_2/5% CO_2 at 34°C for 20 min. Slices were then either incubated in standard recording solution or a high potassium (high K^+) solution for 2–6 h at room temperature, then transferred to standard recording solution until recording. The high K^+ solutions substituted KCl for NaCl, and contained the following (in mM, KCl/NaCl): 52.5:75 for 52 K^+, 26.25:101.25 for 26 K^+, and 13.125:114.375 for 13 K^+. During recordings, 1 µM strychnine was added to block spontaneous glycinergic IPSCs.

Whole-cell patch-clamp recordings were made from BCs in the AVCN using borosilicate patch pipettes of resistance 1.3–2.3 MΩ. Pipettes for voltage-clamp experiments were filled with internal solution containing the following (in mM): 35 CsF, 100 CsCl, 10 EGTA, 10 HEPES, and 1 QX-314, pH 7.3, 300 mOsm. Pipettes for current-clamp experiments were filled with internal solution containing the following (in mM): 130 $KMeSO_3$, 10 NaCl, 2 $MgCl_2$, 0.16 $CaCl_2$, 0.5 EGTA, 10 HEPES, 4 Na_2ATP, 0.4 NaGTP, and 14 Tris-CrPhos, pH 7.2, 302 mOsm. The liquid junction potential was calculated to be 6.6 mV for voltage-clamp and 8.8 mV for current-clamp internal solutions with respect to normal ACSF. Recordings were not corrected for the junction potential. BCs were patched under an Olympus BX51WI microscope with a MultiClamp 700B (Molecular Devices) controlled by an ITC-18 interface (InstruTech), driven by custom-written software (mafPC) running in Igor (WaveMetrics). The bath was perfused at 3–4 ml/min using a pump (403U/VM2; Watson-Marlow), with saline running through an inline heater to maintain the temperature at 34°C (SH-27B with TC-324B controller, Warner Instruments). BCs were held at −70 mV with series resistance 5–15 MΩ compensated to 70%. Cells were identified as BCs by having EPSCs with fast decay kinetics ($\tau <$ 0.2 ms) and half-widths $<$0.5 ms. Single auditory nerve fibers were stimulated using a glass microelectrode placed 30–50 µm away from the soma with 0.2 ms pulses of 4–20 µA through a stimulus isolator (catalog #A360, World Precision Instruments). Single or paired pulses were applied every 8 s. Antagonists used were strychnine (1 µM; catalog #58753, Sigma-Aldrich), (R,S)-CPP (5 µM; catalog #ab120160, Abcam), kynurenate (10 mM; catalog #K3375, Sigma-Aldrich), bicuculline (20 µM; catalog #14340, Sigma-Aldrich), LY367385 (100 µM; catalog #ab120067, Abcam), LY341495 (20 µM; catalog #1209, Tocris Bioscience), MPEP (5 µM; catalog #ab120008, Abcam), CGP55845 (10 µM; catalog #1248, Tocris Bioscience), L-NMMA (500 µM; catalog #ab120137, Abcam, or catalog #0771, Tocris Bioscience), and PKI (1 µM; catalog #476485, Millipore). Agonists used were PAPA-NONOate (300 µM; catalog #ab145196, Abcam), and forskolin (100 µM; catalog #1099, Tocris Bioscience).

Adeno-associated virus neonatal injections. To express optogenetic proteins in auditory nerve fibers, mice ages P2 to P4 were anesthetized using ketamine/xylazine (100:10 mg/kg), and a small incision was made caudal to the pinna to expose the bulla. A 34 gauge needle was inserted into the bulla, and the cochlea was allowed to drain for 10 min. A 5 µl Hamilton syringe was fitted with a 0.375 inch 34 gauge removable needle with 12° bevel, and 0.3 µl of adeno-associated virus (AAV)-syn-ChrimsonR-tdT (catalog #59171-AAV1, Addgene) was injected into the cochlea. After retracting the needle, the skin was sutured, and pups were placed back with their dam for at least 2 weeks before slice preparation. Slices were incubated in standard recording solution at room temperature and exposed to red LED light flashes (625 nm, 40 ms duration, Prizmatix) every 50 ms of 0.4 mW/mm^2, measured with a Thorlabs PM160 meter.

Histology. Slices were prepared from Math5-EYFP mice and from mice injected with pAAV-Syn-ChrimsonR-tdT as for electrophysiology. Slices from mice injected with pAAV-Syn-ChrimsonR-tdT were then drop fixed in 4% buffered paraformaldehyde and postfixed overnight before washing in PBS (0.9% NaCl, 20 mM phosphate buffer, pH 7.4). Slices from Math5-EYFP mice were incubated in normal ACSF or 52 K^+ for at least 4 h, then drop fixed in 4% paraformaldehyde overnight at 4°C. Slices were then incubated in 20% sucrose overnight. Slices were washed three times in PBS, blocked in PBS plus 1% Triton X-100 (PBST) with 5% normal goat serum for 1 h at room temperature, then incubated overnight at 4°C in primary antibody solution containing anti-VGluT1 (polyclonal guinea pig, 1:500; catalog #135304, Synaptic Systems), and anti-GFP (polyclonal rabbit, 1:1000; catalog #A-6455, Invitrogen) in PBST with 1% normal goat serum. Slices were then washed three times in PBS and incubated for 1 h with secondary antibodies Alexa Fluor 488 goat anti-rabbit (1:250; catalog #A-11008, Invitrogen) and Alexa Fluor 594 goat anti-guinea pig (1:250; catalog #A11076, Invitrogen). Finally, all histologic slices were mounted in ProLong Diamond Antifade Mountant (catalog #P36961, Invitrogen) and imaged on an Olympus Fluoview FV1000 confocal.

Auditory brainstem response. Mice were anesthetized with 200 mg/kg ketamine plus 10 mg/kg xylazine and placed on a heating pad (Gaymar) kept at 37°C in a sound booth (Med Associates) lined with Sonex sound-attenuating foam (Acoustical Solutions). Auditory brainstem responses (ABRs) were recorded with a vertex electrode, an electrode inserted behind the pinna ipsilateral to the stimulated ear, and a ground electrode inserted contralateral to the stimulated ear. Clicks (100 µs) were played into the ear canal through a tube from a speaker (MF1, Tucker-Davis Technologies) driven by the Tucker-Davis Technologies ABR rig powered by a WS4 computer with an R26 processor running BioSig software (Tucker-Davis Technologies). ABR threshold was obtained by reducing the stimulus intensity from 90 to 10 dB SPL in steps of 10 dB. ABRs were recorded from the uninjected and injected ears from the same mice.

Experimental design and statistical analysis. Summary statistics are reported throughout as mean ± SEM for normally distributed data and as median ± median absolute deviation for non-normally distributed data. The Shapiro–Wilks test was used to determine normality of each group. The number of cells per group is indicated in the text. Because of the variability in endbulb of Held properties, 15–20 cells were needed for most measurements. The statistical significance level was set at $p < 0.05$, and exact values are shown in the corresponding text. For pairwise comparisons, normally distributed data were compared using Student's *t* test, and nonparametric data were compared using the Mann–Whitney *U* test. For multiple group comparisons, significance was first evaluated using ANOVA (parametric) or Kruskal–Wallis (nonparametric), all of which had $p < 0.01$. For simplicity, therefore, only the results of *post hoc* tests are reported in Results. *Post hoc* tests for normally distributed data were either a Dunnett's test to compare experimental groups to a single control or Tukey's HSD to compare all experimental groups with each other. *Post hoc* tests for non-normally distributed data were either an Anderson–Darling (AD) many-to-one test to compare each group with the control group or an AD all-pairs test to compare all experimental groups to each other. AD tests were implemented in the PMCMRplus package in Rstudio, and used Holm's correction for multiple comparisons. Cluster analysis was done by hclust in Rstudio using the complete linkage method after normalizing $EPSC_1$ and PPR values to zero mean and unit variance.

Results

Effects of high K^+

We developed an *in vitro* preparation to mimic high levels of acoustically driven activity in auditory nerve fibers by exposing acute slices of the AVCN to solutions with potassium concentrations up to 52 mM. We evaluated the acute effects by making voltage-clamp recordings from BCs during high K^+ treatment. Larger holding currents were required during treatment with high K^+ (Fig. 1*Ai*, top). In addition, BCs showed increased presynaptic activity, particularly above 26 K^+ (Fig. 1*Aii–v*). The amplitudes of synaptic events appeared larger than the typical mEPSC amplitude at the endbulb (50–100 pA) but smaller than the typical evoked EPSC (5–10 nA; Isaacson and Walmsley, 1996; Oleskevich and Walmsley, 2002; Chanda and Xu-Friedman, 2010). We could not practically distinguish individual events because of their high rates, so we quantified activity using the variance of the holding current, which increased substantially in 52 K^+ (Fig. 1*Ai*, bottom, 1*B*). We also evaluated the effect of high K^+ treatment in current clamp and found strong depolarization with all high K^+ solutions (Fig. 1*C*), to ~40 mV in 52 K^+ (Fig. 1*D*). Thus, high K^+ was effective at increasing activity.

There was some concern that exposure to high K^+ might be toxic to BCs and endbulbs. Acute brain slices are normally quite variable in health, and visual inspection suggested that slices incubated in normal ACSF or high K^+ for several hours had similar numbers of cells available for patching. To investigate this further, we assessed cell health qualitatively by preparing acute slices from Math5-EYFP mice, in which BCs express yellow fluorescent protein (Kronander et al., 2017), and then incubating slices in either normal ACSF or 52 K^+. We then fixed the slices and visualized endbulbs by immunostaining for VGluT1. We found BCs and endbulbs of varying apparent health in both samples, with similar numbers of intact BCs surrounded by endbulbs (Fig. 2*A*,*B*, white arrows, 2*C*,*D*, magnified examples). Thus, it does not appear that 52 K^+ treatment is particularly toxic to BCs or endbulbs.

We assessed the consequences of high K^+ treatment on synaptic function by returning slices to normal ACSF and evoking EPSCs from auditory nerve fibers. Without high K^+ treatment,

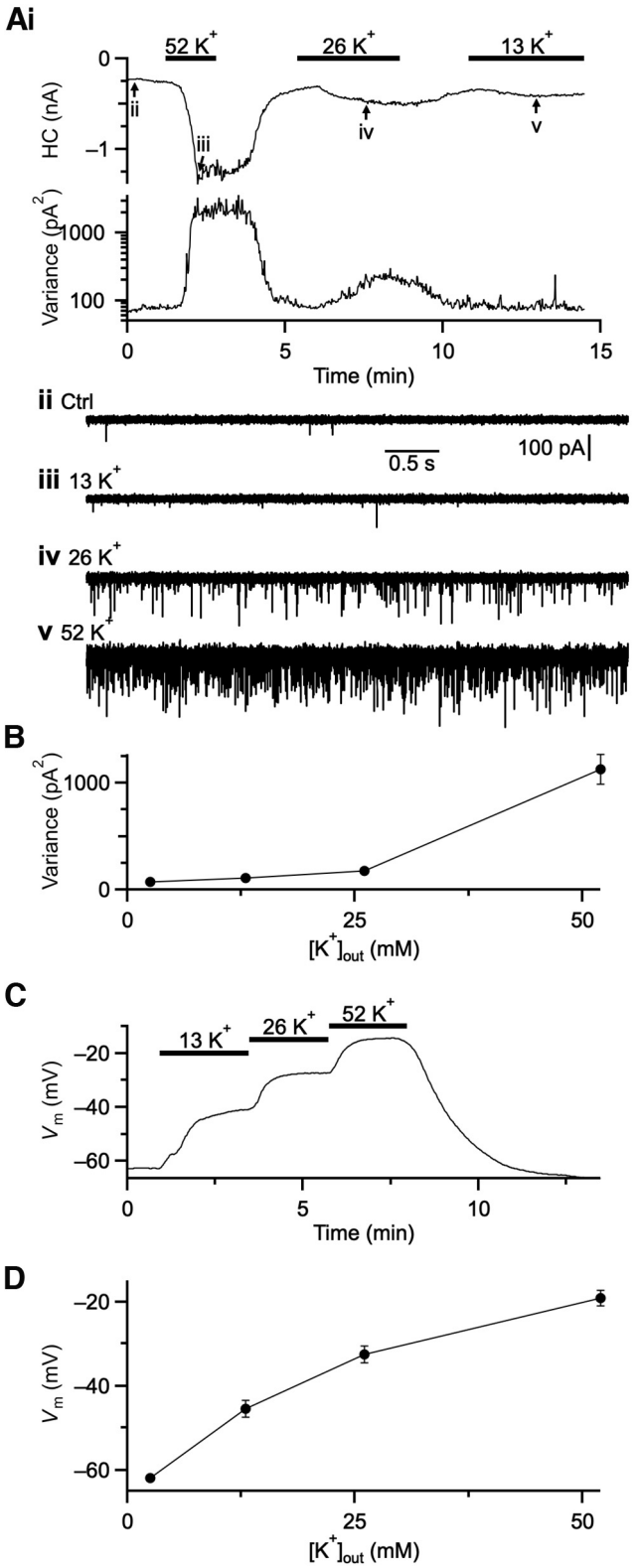

Figure 1. Acute effects of high K^+ treatment. ***A***, Representative voltage-clamp recording, showing (***i***) mean (top) and variance (bottom) of holding current, and (***ii–v***) traces recorded at times indicated in ***i***. ***B***, Variance of holding current increases with high K^+. Points are averages of 10–21 experiments. ***C***, Representative current-clamp recording showing resting membrane potential in different K^+ concentrations. ***D***, Resting membrane potential depolarizes with high K^+. Points are averages of five experiments.

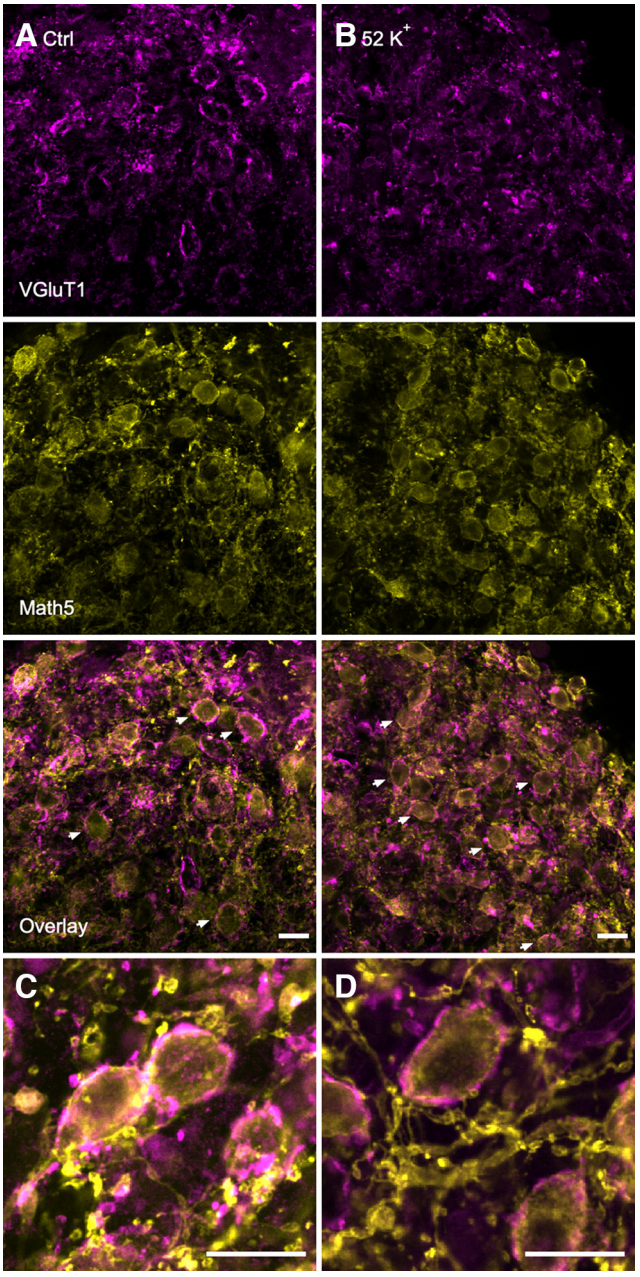

Figure 2. Slice quality following high K^+ treatment. ***A***, ***B***, Representative images of VGluT1-immunolabelled endbulbs (top, magenta) and Math5-EYFP BCs (middle, yellow) following 4 h incubation in normal ACSF (***A***) or 52 K^+ (***B***). Intact BCs with endbulbs are indicated with white arrows in the bottom row. ***C***, ***D***, Enlarged images of intact BCs with endbulbs after incubation in normal ACSF (***C***) or 52 K^+ (***D***). Images are single confocal sections. Scale bars: 20 µm.

EPSC amplitudes were 6.0 ± 2.9 nA (median ± median absolute deviation for EPSC amplitudes throughout, 21 cells; Fig. 3*A*,*B*, black markers). EPSC amplitude decreased significantly after a 4 h treatment with 26 K^+ (2.2 ± 1.0 nA, 21 cells, $p = 0.009$, AD many-to-one test, violet markers) and 52 K^+ (1.2 ± 0.6 nA, 16 cells, $p < 0.001$, red markers), with a marginal decrease in 13 K^+ (3.8 ± 1.6 nA, 11 cells, $p = 0.15$, blue markers; Fig. 3*A*,*B*). Exposure to 52 K^+ for <4 h did not produce a significant change from control (0.1–2 h, 7.6 ± 2.6 nA, 12 cells, $p = 0.29$; 2.1–4 h, 1.7 ± 1.1 nA, 10 cells, $p = 0.06$; AD tests; Fig. 3*C*, black vs red markers).

The amplitude of the EPSC is influenced by the underlying synaptic properties P_r and quantal size Q (Regehr and Stevens, 2001). To assess changes in P_r, we evoked pairs of EPSCs with a 3 ms interval (Fig. 3*A*) and calculated the paired-pulse ratio (PPR = $EPSC_2$/$EPSC_1$), which was 0.55 ± 0.04 in control synapses (mean ± SEM for PPRs throughout, 21 cells). PPR is sensitive to changes in P_r, where an increase in P_r is reflected as a smaller PPR, and a decrease in P_r is reflected as a larger PPR. PPR increased significantly after incubating slices for at least 4 h in all K^+ concentrations (13 K^+ = 0.72 ± 0.05, 11 cells, blue markers; 26 K^+ = 0.73 ± 0.04, 19 cells, violet markers; 52 K^+ = 0.92 ± 0.04, 16 cells, red markers; $p < 0.02$ each comparison to control, Dunnett's tests; Fig. 3*B*). Furthermore, significant changes in PPR in 52 K^+ required at least 4 h incubation (0.1–2 h, 0.45 ± 0.06, 12 cells; 2.1–4 h, 0.68 ± 0.11, 10 cells; $p > 0.2$ all comparisons to control, Dunnett's test; Fig. 3*D*, red vs black markers). The increase in PPR (i.e., lower P_r) after treatment with 52 K^+ was consistent with smaller $EPSC_1$ in Figure 3*A*–*C*. Furthermore, smaller $EPSC_1$ and higher PPR are also observed at endbulbs after 1–2 d noise exposure *in vivo* (Wong and Xu-Friedman, 2022). Therefore, treatment with 52 K^+ appears to mimic the effects of noise exposure, and we incubated for at least 4 h in 52 K^+ for subsequent experiments.

We assessed the effects of high K^+ on Q by measuring spontaneous EPSCs (Fig. 3*E*,*F*). Auditory nerve fibers do not spontaneously fire action potentials in acute slices, so spontaneous EPSCs result from fusion of single quanta and are therefore equivalent to mEPSCs. In control BCs, mEPSC amplitude was 102.8 ± 22.1 pA (median ± median absolute deviation, 14 cells; Fig. 3*G*, black markers). After 4 h in 52 K^+, mEPSC amplitude decreased significantly (69.2 ± 10.5 pA, 9 cells, $p = 0.03$, Mann–Whitney U; Fig. 3*G*, red markers). Previously, we found that Q did not change after noise exposure or conductive hearing loss *in vivo* (Ngodup et al., 2015; Zhuang et al., 2017; Wong and Xu-Friedman, 2022), so this decrease *in vitro* was surprising and likely contributed to the decrease in $EPSC_1$ amplitude in Figure 3, *A*–*C*. We did not observe a significant change in mEPSC frequency (control = 4.3 ± 2.0 s^{-1}; 52 K^+ = 8.7 ± 1.6 s^{-1}; median ± median absolute deviation, $p = 0.31$, Mann–Whitney U; Fig. 3*H*). Frequency of mEPSCs is thought to depend on the number of release sites, so changes in N are unlikely with this paradigm.

Signaling mechanisms

We next investigated the signaling mechanisms causing synaptic changes by coapplying 52 K^+ with antagonists against candidate signaling pathways. We reasoned that if a candidate molecule played a role in induction, then coapplication of its antagonist would yield a significant difference in $EPSC_1$ amplitude and PPR compared with the effects of 52 K^+ alone. To avoid false positives, we performed statistical comparisons correcting for multiple comparisons across all antagonists in Figure 4, *A*–*C*, but we describe the results step by step here for clarity. Figure 4*A* shows $EPSC_1$ and PPR following coapplication of 52 K^+ with the NMDA receptor antagonist CPP (three cells, blue markers), the AMPA and NMDA receptor antagonist kynurenate (three cells, violet markers), and a combination of the $GABA_A$ receptor antagonist bicuculline plus the glycine receptor antagonist strychnine plus kynurenate (four cells, pink markers). None of the three treatments showed a significant difference from 52 K^+ alone ($EPSC_1$, AD tests; PPR, Dunnett's tests; $p > 0.34$ all comparisons). This indicates that high K^+ does not reduce $EPSC_1$ and P_r through activation of AMPA, NMDA, $GABA_A$, or glycine receptors.

In addition, blocking multiple metabotropic receptor signaling pathways did not prevent the effects of 52 K^+ treatment.

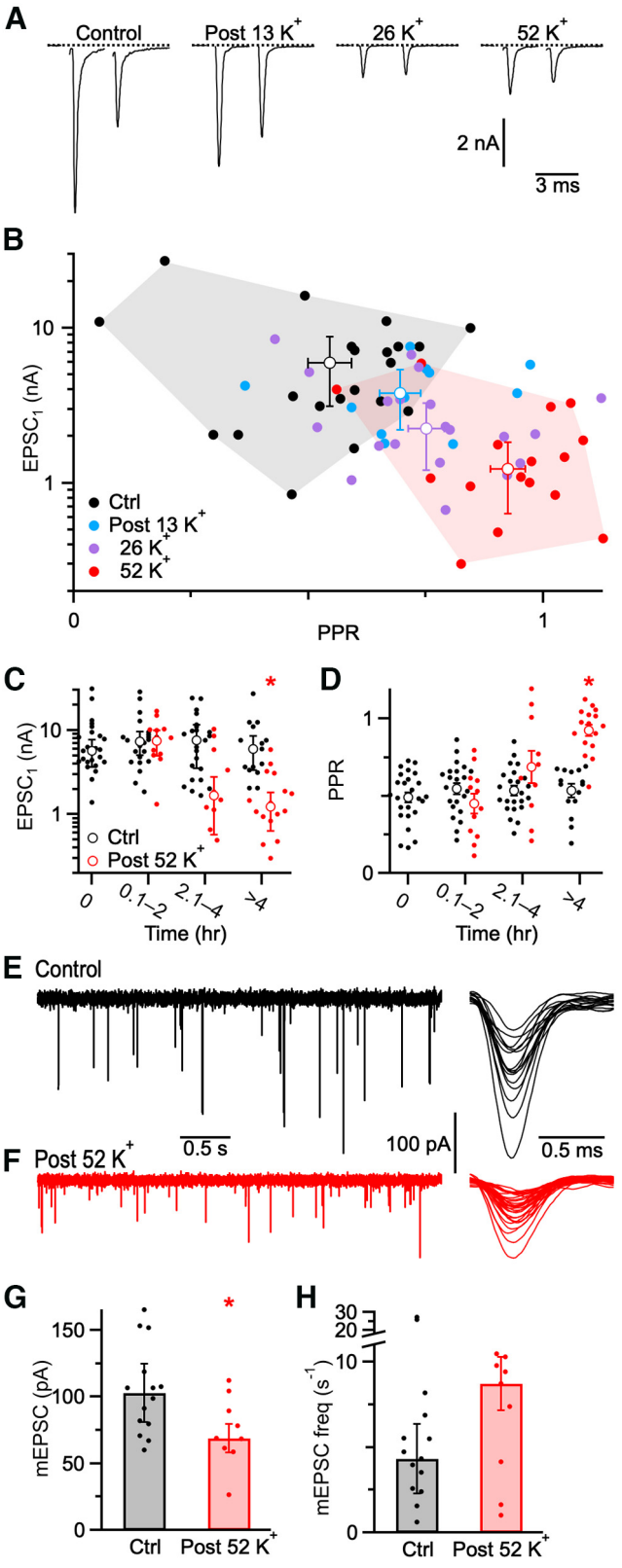

Figure 3. Treatment with high K^+ solution reduces EPSC amplitude, release probability, and quantal size. ***A***, Representative pairs of evoked EPSCs in control endbulbs and after incubation in 13, 26, and 52 K^+ for >4 h and return to normal ACSF. ***B***, $EPSC_1$ amplitude and PPR for individual endbulbs following treatment with high K^+. Solid symbols are individual experiments, and open symbols are averages. ***C***, ***D***, Time course of changes in $EPSC_1$ amplitude (***C***) and PPR (***D***) following treatment with 52 K^+. Dots are individual experiments, and open circles are averages. ***E***, ***F***, Spontaneous mEPSCs recorded in control BCs (***E***) and after incubation in 52 K^+ for 4 h (***F***). Individual mEPSCs are overlaid and expanded at right. ***G***, ***H***, Effects of 52 K^+ on average mEPSC amplitude (***G***) and frequency (***H***). Average effects are depicted throughout as mean ± SEM. Asterisks (*) denote significance at $p < 0.05$.

Figure 4*B* shows $EPSC_1$ and PPR after coapplication of 52 K^+ with antagonists against group I (LY367385, MPEP, six cells, blue markers) or group II (LY341495, three cells, violet markers) mGluRs. Green markers show $EPSC_1$ and PPR after treatment of acute slices from CB1R knock-out mice with 52 K^+ (eight cells; Fig. 4*B*). Orange markers show $EPSC_1$ amplitude and PPR after induction with 52 K^+ and subsequent treatment with the $GABA_B$ receptor antagonist CGP55845 (five cells; Fig. 4*B*). None of these antagonists showed a significant difference in $EPSC_1$ or PPR compared with treatment with 52 K^+ alone ($EPSC_1$, AD tests; PPR, Dunnett's tests; $p > 0.5$ all comparisons). Thus, high K^+ does not appear to reduce P_r through activation of $GABA_B$ receptors, CB1Rs, or group I or group II mGluRs.

We also considered two additional molecules that modulate synaptic properties, NO and protein kinase A (PKA). NO influences multiple cells and synapses in the auditory brainstem (Steinert et al., 2008; Cao et al., 2019) but has no known role at auditory nerve synapses. We tested the role of NO by coapplying 52 K^+ with the neuronal nitric oxide synthase (nNOS) inhibitor L-NMMA. In this case, PPR was significantly more depressed compared with 52 K^+ alone (0.73 ± 0.05, five cells, $p = 0.04$, Dunnett's test), although $EPSC_1$ amplitude was not significantly greater (2.0 ± 1.5 nA, five cells, $p > 0.5$, AD test; Fig. 4*C*, orange markers). PKA is involved in a host of signaling pathways, including modulating P_r at some synapses (Chen and Regehr, 1997). When 52 K^+ was coapplied with the PKA inhibitor PKI, PPR was not significantly different from 52 K^+ alone (0.80 ± 0.05, nine cells, $p = 0.23$, Dunnett's test), and $EPSC_1$ amplitude was larger, but not significantly so (3.9 ± 1.5 nA, nine cells, $p = 0.16$, AD test; Fig. 4*C*, blue markers). Because L-NMMA and PKI appeared to each have partial effects, we coapplied 52 K^+ with both L-NMMA and PKI, which fully prevented the effects of 52 K^+ alone on PPR (0.65 ± 0.05, seven cells, $p < 0.001$, Dunnett's test), and $EPSC_1$ amplitude (6.3 ± 2.9 nA, seven cells, $p = 0.007$, AD test; Fig. 4*C*, pink markers). This suggests that high K^+ acts via both NO and PKA to reduce P_r and $EPSC_1$.

We verified the involvement of NO in inducing synaptic changes by treating slices with the NO donor PAPA-NONOate for at least 2 h without 52 K^+, then assessing EPSCs in control ACSF. PAPA-NONOate caused a significant increase in PPR (0.79 ± 0.04, 16 cells; $p < 0.001$, *t* test) and decrease in $EPSC_1$ amplitude (2.2 ± 1.0 nA, 16 cells, $p = 0.02$, Mann–Whitney *U*; Fig. 4*D*, blue markers). This shows that NO is sufficient to induce synaptic changes. In addition, these experiments act as important controls that 52 K^+ does not reduce P_r through some nonspecific mechanism, such as by injuring synaptic function. Rather, 52 K^+ activates cellular pathways involving NO and PKA that specifically downregulate neurotransmitter release in auditory nerve synapses.

Treatment with 52 K^+ versus noise exposure

We wanted to know whether noise exposure *in vivo* and treatment with 52 K^+ *in vitro* induced synaptic changes through the same mechanism. To test this, we first exposed mice to noise for at least 7 d, which produced significantly higher PPR (0.72 ± 0.07, $p = 0.04$, Tukey's test), and $EPSC_1$ amplitude similar to control (5.9 ± 2.6 nA, 14 cells, $p = 0.97$, AD test; Fig. 5*A*), consistent with our previous findings (Ngodup et al., 2015). When we

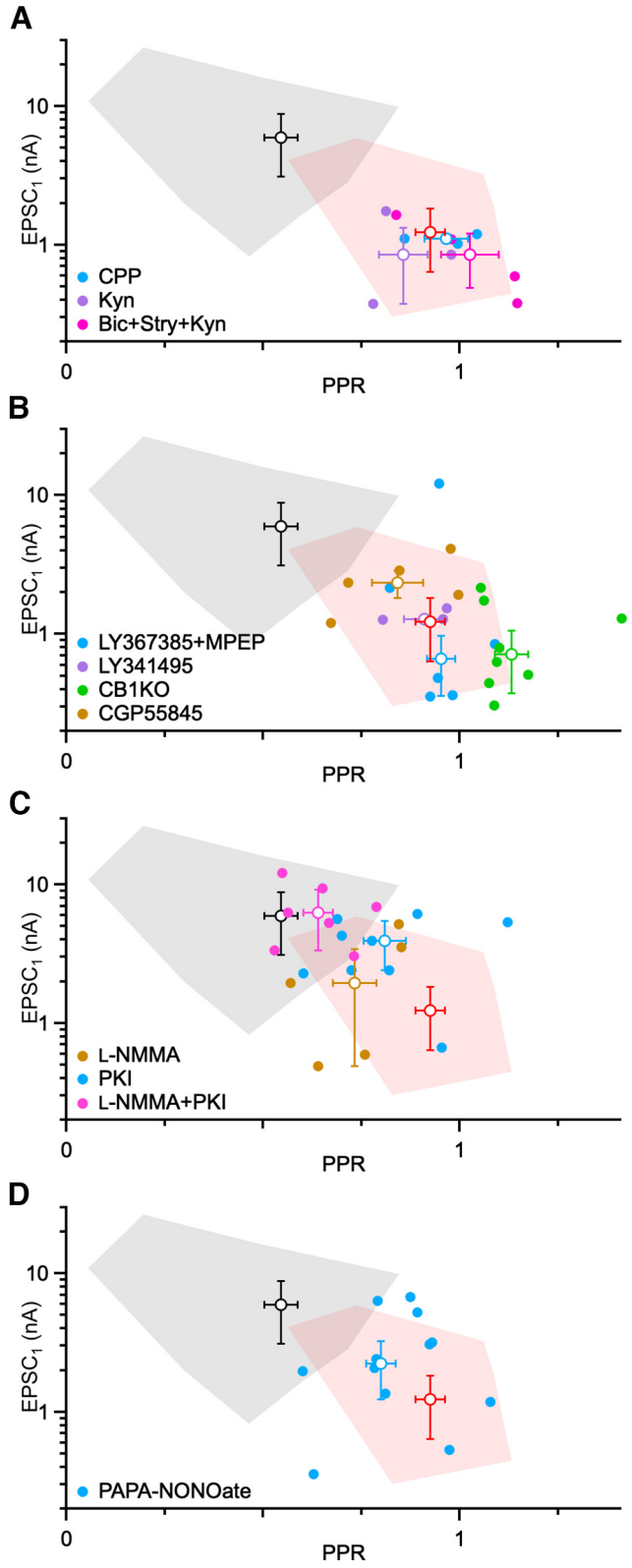

Figure 4. Testing candidate signaling pathways for induction of synaptic changes by 52 K^+. EPSC measurements were made after returning to normal ACSF. ***A***, Ionotropic receptors. Closed markers indicate $EPSC_1$ amplitude and PPR of individual endbulbs following treatment with 52 K^+ in the presence of CPP, kynurenate, or bicuculline plus strychnine plus kynurenate. Open markers indicate average effects. ***B***, Metabotropic receptors. Closed markers indicate $EPSC_1$ amplitude and PPR of individual endbulbs following treatment with 52 K^+ in the presence of group I mGluR antagonists LY367385 and MPEP and group II mGluR antagonist LY341495. Green markers are $EPSC_1$ and PPR of individual endbulbs in CB1R KO mice following treatment with 52 K^+. Orange markers are $EPSC_1$ and PPR of individual endbulbs treated with 52 K^+, then treated acutely with $GABA_B$-receptor antagonist CGP55845. ***C***, $EPSC_1$ amplitude and PPR of endbulbs following treatment with 52 K^+ in the presence of NOS antagonist L-NMMA, PKA antagonist PKI, and both antagonists combined. ***D***, $EPSC_1$ amplitude and PPR for endbulbs following treatment with the NO donor PAPA-NONOate. Solid symbols in ***A–D*** are individual experiments, and open symbols are averages ± SEM. The average and range of values for control (black circle, gray shading) and 52 K^+ (red circle, pink shading) are duplicated from Figure 3 for comparison. Markers in the shaded pink region reflect normal induction and in the gray region reflect no induction.

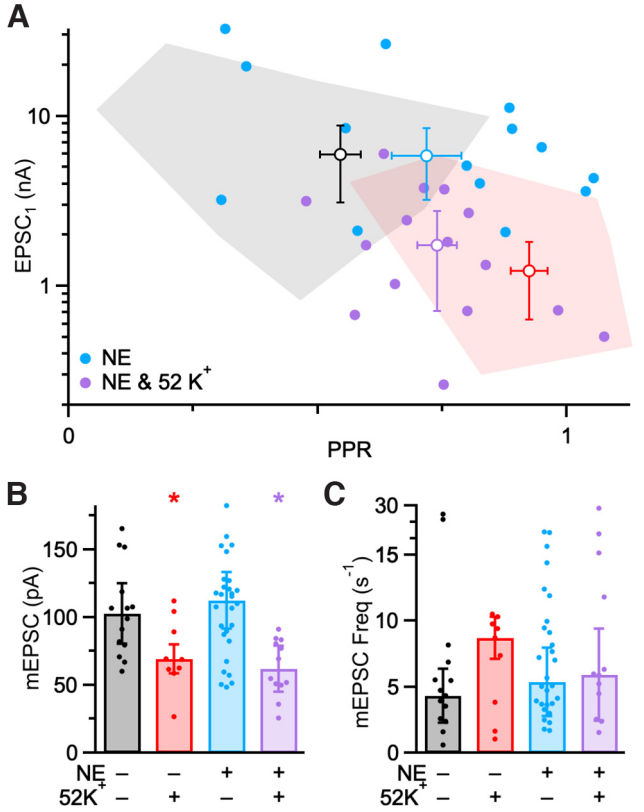

Figure 5. Effects of 52 K^+ on noise-exposed endbulbs. EPSC measurements were made after returning to normal ACSF. ***A***, $EPSC_1$ amplitude and PPR of endbulbs from noise-exposed animals and following further treatment with high K^+. Solid symbols are individual experiments, and open symbols are averages ± SEM. The average and range of values for control (black circle, gray shading) and 52 K^+ (red circle, pink shading) are duplicated from Figure 3 for comparison. ***B***, ***C***, Effects of noise exposure and 52 K^+ on mEPSC amplitude (***B***) and frequency (***C***). Effects of 52 K^+ on control synapses are repeated from Figure 3 for comparison.

treated slices from noise-exposed mice with 52 K^+, PPR did not change further (0.74 ± 0.04, 15 cells, $p = 0.86$, Tukey's test), but $EPSC_1$ amplitude decreased significantly (1.7 ± 1.0 nA, $p < 0.001$, AD test; Fig. 5*A*, purple markers).

To determine how $EPSC_1$ decreased with no change in P_r, we assessed changes in Q using mEPSCs. The amplitude of mEPSCs from noise-reared mice was 112.8 ± 21.0 pA (29 cells, blue symbols; Fig. 5*B*), and frequency was 5.4 ± 2.6 s^{-1} (Fig. 5*C*). After additional treatment with 52 K^+, mEPSC amplitude decreased significantly (62.0 ± 17.0 pA, 12 cells, violet symbols, $p < 0.001$, Tukey's test; Fig. 5*B*) with no significant change in mEPSC frequency (5.9 ± 3.5 s^{-1}, 12 cells, $p > 0.50$, AD test; Fig. 5*C*). Thus, the smaller $EPSC_1$ amplitude following 52 K^+ treatment in noise-exposed endbulbs could result from decreased Q. Together, these results indicate that noise exposure occludes further changes in P_r resulting from treatment with

←

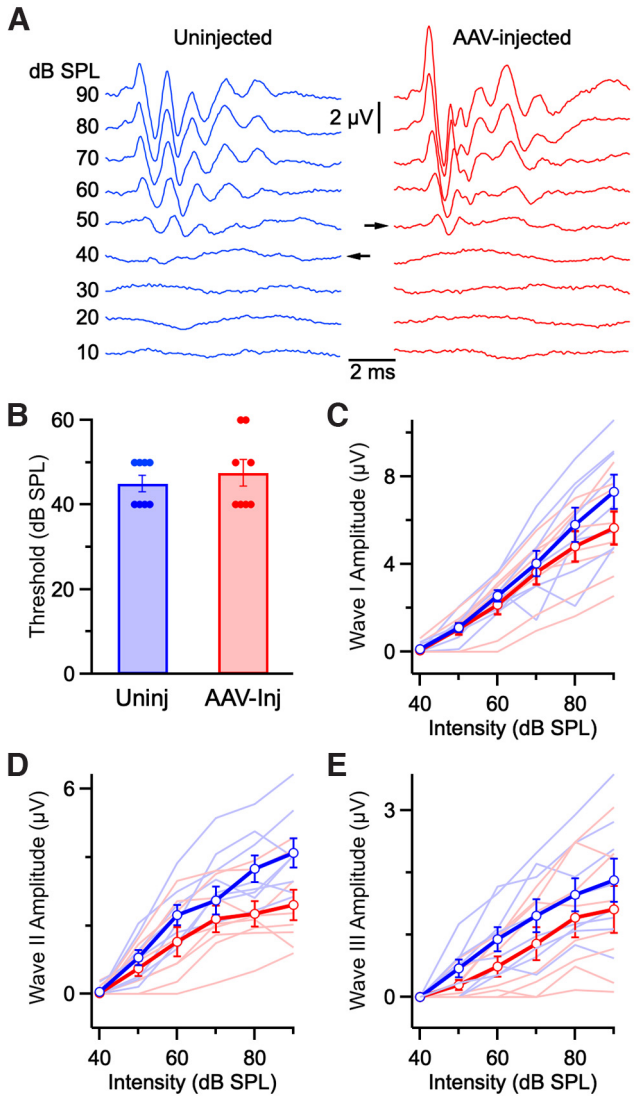

Figure 6. Effects of round window injections of AAVs on auditory brainstem responses (ABRs). ***A***, Representative ABRs from uninjected (blue) and AAV-injected (red) ears. Uninj, Uninjected; Inj, injected. ***B***, Average ABR thresholds from ears of uninjected (8 ears) and AAV-injected mice (8 ears). There was no significant difference between the two groups ($p > 0.50$, paired t test). ***C–E***, Peak amplitudes of ABR waves I (***C***), II (***D***), and III (***E***) for clicks of different intensities. The slopes differed significantly for wave II ($p = 0.03$, t test), but not wave III ($p = 0.65$), and were on the edge of significant for wave I ($p = 0.06$).

52 K^+, suggesting they share underlying cellular mechanisms. By contrast, 52 K^+ modulates Q through pathways not occluded by noise exposure.

Elevating activity with optogenetics

To determine how increased activity drives NO release, we turned to optogenetics to activate auditory nerve fibers specifically. We expressed ChrimsonR in auditory nerve fibers by injecting AAV-ChrimsonR-tdTomato through the round window of P2–P4 mice and allowing at least 2 weeks incubation. We assessed possible deleterious effects of injection or ChrimsonR expression by measuring ABRs from injected and uninjected ears (Fig. 6*A*). ABRs from both groups had similar thresholds (uninjected 45 ± 2 dB SPL vs injected 47 ± 3 dB SPL, eight ears each, $p = 0.52$, paired t test; Fig. 6*B*). We also assessed suprathreshold ABRs by comparing slopes of individual ABR wave amplitudes as a function of click intensity. AAV injection caused a marginal change in wave I (uninjected 156 ± 18 nV/dB vs injected 108 ± 18 nV/dB, $p = 0.06$, t test; Fig. 6*C*) and no detectable change in wave III (uninjected 35 ± 8 nV/dB vs injected 30 ± 9 nV/dB, $p = 0.65$; Fig. 6*E*). but there was a significantly lower slope for wave II (uninjected 75 ± 11 nV/dB vs injected 37 ± 12 nV/dB, $p = 0.03$, t test; Fig. 6*D*). Wave II likely corresponds to activity in the cochlear nucleus (Rüttiger et al., 2017), so injection or virus expression may have affected activity somewhat in the AVCN *in vivo*, which by itself could have consequences for $EPSC_1$ amplitude or PPR.

We used optogenetic stimulation after P18, when auditory nerve afferents and endbulbs showed strong labeling (Fig. 7*A*). In acute slices from ChrimsonR-injected mice, strobing with a red LED at 20 Hz reliably drove EPSCs in voltage clamp and triggered postsynaptic action potentials in current clamp (Fig. 7*B*). Therefore, we used optogenetic stimulation to drive activity, specifically in auditory nerve fibers, by strobing brain slices at 20 Hz (40 ms light pulses). After 2 h of strobing, tdTomato fluorescence was no longer visible, and ChrimsonR activity appeared to be depleted, so we could not specifically identify BCs receiving infected synapses and target them for recording. Instead, we recorded from any healthy BCs and stimulated individual presynaptic auditory nerve fibers electrically. This population likely included fibers that did and did not express ChrimsonR and so may or may not have been optogenetically stimulated.

We measured $EPSC_1$ amplitude and PPR after strobing for 2 h (22 cells, 6 mice), and the results were multimodal. We performed hierarchical cluster analysis, and found $EPSC_1$ and PPR data fell into three clusters (Fig. 7*C*). Cluster 1 (C1; 12 cells, 55%) had an average PPR that was not significantly different from unstrobed controls (0.48 ± 0.06, $p = 0.95$, Tukey's test), and an $EPSC_1$ amplitude that was lower but not significantly so (3.0 ± 0.7 nA, $p = 0.51$, AD test; Fig. 7*C*, pink markers). Thus, Cluster 1 appeared to be synapses that were insensitive to strobing. By contrast, Cluster 2 (C2; 9 cells, 41%) exhibited significantly higher PPR (0.98 ± 0.03, $p < 0.001$, Tukey's test) and smaller $EPSC_1$ amplitude (0.64 ± 0.53 nA, $p = 0.002$, AD test; Fig. 7*C*, blue markers). Furthermore, the PPR and $EPSC_1$ of Cluster 2 were similar to synapses after 52 K^+ treatment (PPR, $p = 0.98$, Tukey's test; $EPSC_1$, $p = 0.51$, AD test). We interpreted Cluster 2 to be synapses that were activated by strobing and underwent long-term synaptic changes. Cluster 3 (C3) consisted of a single point (Fig. 7*C*, orange marker), so it was not considered further. Strikingly, a cumulative frequency plot of PPR from all strobed synapses (Fig. 7*E*, dotted black line) showed highly depressing synapses similar to control (solid black line), as well as nondepressing synapses similar to 52 K^+ (red line), underscoring the interpretation that strobing drove a decrease in P_r in a subset of cells.

We also investigated whether changes in Q might contribute to smaller $EPSC_1$ amplitude. Amplitudes and frequencies of mEPSCs did not differ between the two clusters (Cluster 1 = 97.3 ± 21.2 pA, 3.6 ± 2.5 s^{-1}, pink markers; Cluster 2 = 90.1 ± 29.0 pA, 1.5 ± 0.7 s^{-1}, blue markers; $p > 0.2$, Mann–Whitney U, both comparisons; Fig. 7*C*, inset). This differs from 52 K^+ treatment, which drove a decrease in mEPSC amplitude (Fig. 7*C*, inset, red markers). Thus, optogenetic strobing appears more similar to the effects of noise exposure *in vivo*, where P_r and EPSC amplitude decrease but Q does not.

We used the optogenetic model to investigate the role of postsynaptic ionotropic glutamate receptor activation in NO release. Patch-clamp recordings verified that kynurenate (10 mM) fully blocked postsynaptic AMPA and NMDA receptor activation during strobing, which was fully reversible. When kynurenate

was applied during strobing, subsequent measurements of PPR (0.53 ± 0.05, 12 cells; Fig. 7*D*, pink markers) and $EPSC_1$ (2.6 ± 1.5 nA) were not significantly different from Cluster 1 ($p > 0.99$, both comparisons, Tukey's and AD tests), but PPR was significantly different from Cluster 2 ($p < 0.001$, Tukey's test; Fig. 7*D*). This suggests that synaptic changes require activation of postsynaptic ionotropic glutamate receptors, and strobing itself does not induce nonspecific synaptic changes, such as through presynaptic excitotoxicity.

We tested the role of NMDA receptors specifically by strobing slices in the presence of CPP, which led to a wide range of $EPSC_1$ and PPR (Fig. 7*D*, blue markers). Of 14 cells, four (30%) had $EPSC_1$ and PPR within the range of control, uninfected synapses, similar to Cluster 1 in Figure 7*C*. We interpret these as a combination of synapses that did not express ChrimsonR and synapses that required NMDA receptor activation to induce synaptic changes. The remaining cells (70%) showed elevated PPR and decreased $EPSC_1$ amplitude within the range of synapses treated with 52 K^+. PPR of all cells differed significantly from both Cluster 1 and Cluster 2 ($p < 0.02$ both comparisons, Tukey's tests; Fig. 7*E*), indicating that synapses were affected by strobing, but changes were weaker in the presence of CPP. Thus, strobing appears to induce synaptic changes partially through activation of AMPA receptors, with the full effects requiring NMDA receptor activation.

We verified that the signaling pathway activated by optogenetic stimulation acted through NOS by applying L-NMMA during strobing. We found that the PPR was not significantly different from control (0.48 ± 0.03, $p = 0.94$, 9 cells, Tukey's test; Fig. 7*E*, green vs black lines). This suggests that synaptic changes driven by strobing also require NOS, similar to what we observed with 52 K^+, suggesting both induction methods act on the same signaling pathway.

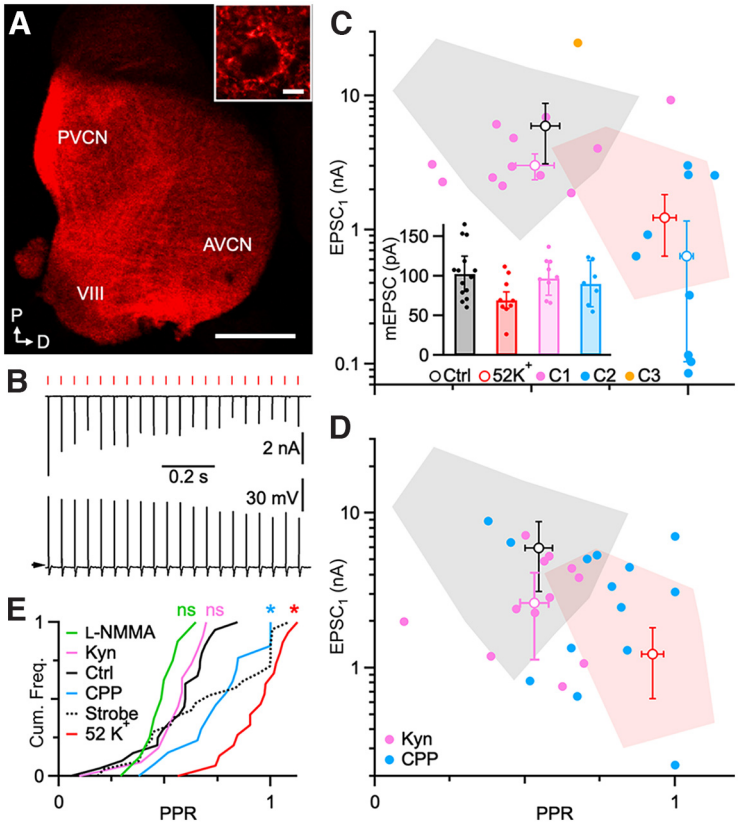

Figure 7. Induction using optogenetics reveals role of postsynaptic AMPA and NMDA receptors. ***A***, Sagittal section of the cochlear nucleus showing expression of ChrimsonR-tdTomato in auditory nerve fibers after round-window injection. Inset, Magnified view of a labeled endbulb. Scale bars: 100 µm; inset, 10 µm. Arrows indicate approximate posterior and dorsal directions. ***B***, Representative EPSCs in voltage-clamp (top trace) and postsynaptic action potentials in current clamp (bottom trace) evoked by 20 Hz flashes of red light (top red markers). Arrow on current-clamp trace indicates −60 mV. ***C***, $EPSC_1$ amplitude and PPR for endbulbs following strobing for ≥2 h. Solid symbols are individual endbulbs with colors according to cluster analysis, and open symbols are averages. Inset, Amplitude of mEPSCs does not decrease following strobing. ***D***, $EPSC_1$ amplitude and PPR for endbulbs strobed in the presence of glutamate receptor antagonists kynurenate and CPP. The average and range of values for control (black circles, gray shading) and 52 K^+ (red circles, pink shading) in ***C*** and ***D*** are duplicated from Figure 3 for comparison. Markers in the shaded pink region reflect normal induction and in the gray region reflect no induction. ***E***, Cumulative frequency histogram of PPR following strobing and with kynurenate, CPP, or L-NMMA. Asterisks (*) denote significance at $p < 0.05$; ns denotes not significant.

Discussion

We demonstrated that elevating activity in the AVCN *in vitro* leads to reduced probability of neurotransmitter release at auditory nerve synapses in a few hours. Optogenetic experiments revealed that induction of presynaptic changes by auditory nerve activity requires activation of both AMPA and NMDA receptors. Prolonged depolarization using high K^+ can also induce presynaptic changes through NO. Together, our results suggest that high activity in auditory nerve fibers drives activation of postsynaptic AMPA and NMDA receptors, depolarization of postsynaptic cells, activation of NOS, and release of NO onto endbulbs to induce a decrease in P_r. These experiments reveal that auditory nerve synapses are unexpectedly labile, showing a presynaptic form of long-term depression, surprisingly similar to synapses associated with learning and memory.

Nitric oxide signaling

Our experiments indicate that synaptic changes are driven by activation of NOS and release of NO. NOS and NO have been linked to induction of long-term plasticity in other systems *in vitro* (Daniel et al., 1993; Jacoby et al., 2001; Bon and Garthwaite, 2003; Qiu and Knöpfel, 2007) and *in vivo* (Dachtler et al., 2011). In the AVCN, NOS is expressed by bushy and stellate cells, as well as terminals of the auditory nerve (Burette et al., 2001; Coomber et al., 2015). The NOS implicated here is most likely localized to postsynaptic cells, because the strobe experiments indicated that AMPA and NMDA receptors were necessary for induction. Additional experiments will be needed to identify the specific postsynaptic cell type, whether BCs, stellate cells, or glial cells. Furthermore, NO is well known to serve as a retrograde messenger in other synapses (Arancio et al., 1996; Regehr et al., 2009).

Activation of NOS commonly depends on rises in intracellular Ca (Bredt and Snyder, 1990), which could result from influx through NMDA receptors (Qiu and Knöpfel, 2007; Olthof et al., 2019), Ca-permeable AMPA receptors (Wang et al., 1998; Gardner et al., 1999; Haj-Dahmane et al., 2017), or postsynaptic voltage-gated Ca channels that open during synaptic activity. In BCs, the current through NMDA receptors can be small (Bellingham et al., 1998) but increases substantially during periods of high activity (Pliss et al., 2009). In the high K^+ experiments, glutamate receptors

were not required to induce synaptic changes, most likely because postsynaptic cells were directly depolarized, suggesting that voltage-gated Ca channels are also important.

An important question is the precision of NO signaling. NO could be precisely targeted, signaling from an activated bushy cell to a single active endbulb. Alternatively, the NO could be released by a bushy cell to modulate all its presynaptic endbulbs. This could relate to the finding that auditory nerve synapses that converge on the same bushy cell appear to have similar P_r (Yang and Xu-Friedman, 2012). This is surprising, because converging auditory nerve fibers include multiple subtypes with diverse individual activity levels (Wang et al., 2021). If NO release from a bushy cell signals to all its converging inputs simultaneously, that may have the effect of coordinating their P_r. Another possibility is that NO acts on many endbulbs and BCs in wider regions of the AVCN as a volume transmitter. NO is released by neighbors of BCs in the AVCN, T-stellate cells, which transiently enhances presynaptic inputs to the T-stellate cells (Cao et al., 2019). Acute treatment with NO donors and antagonists affects activity in the AVCN *in vivo* (Hockley et al., 2020). NO also regulates postsynaptic excitability in other auditory nuclei, the medial nucleus of the trapezoid body (Steinert et al., 2008) and the superior paraolivary nucleus (Yassin et al., 2014). Ours is the first evidence that NO acts on auditory nerve synapses.

Our experiments also indicated a role for PKA in inducing synaptic changes as the antagonist PKI partially prevented the induction of lower P_r by 52 K^+. PKA is associated with modulating P_r in other systems (Chen and Regehr, 1997; Huang and Kandel, 1998; Fourcaudot et al., 2008; Bender et al., 2009). The efficacy of PKI was greater in combination with NOS antagonists. This could occur if NOS and PKA are in the same signaling pathway (Qiu and Knöpfel, 2007), but each antagonist is only partially effective. Alternatively, NOS and PKA may be in two separate signaling pathways that each partially modulate P_r. More work will be needed to determine how NOS and PKA interact to drive activity-dependent changes in P_r at auditory nerve synapses.

Relationship to noise exposure in vivo

Our data support that the induction mechanisms investigated here are responsible for activity-dependent changes in P_r *in vivo* (Ngodup et al., 2015). For endbulbs already exposed to noise, subsequent treatment with high K^+ did not induce a further increase in PPR; that is, changes in P_r were occluded. One major difference is that noise exposure *in vivo* requires 1–2 d before measurable synaptic changes are observed (Wong and Xu-Friedman, 2022), whereas 52 K^+ induced synaptic changes in 4–6 h and strobing in only 2 h. Strobing may have high efficacy because it presumably drives auditory nerve activity synchronously throughout the slice, possibly leading to high peak concentrations of NO. Noise exposure *in vivo* probably also activates many auditory nerve fibers but less synchronously, so NO levels may be lower. High K^+ produced considerable depolarization but few action potentials, most likely because of sodium channel inactivation. Thus, the presence and timing of action potentials may be important in driving the release of NO.

Our data suggest additional homeostatic mechanisms may also play a role *in vivo*. Treatment with high K^+ caused a 40% decrease in quantal size, Q, which resembles homeostatic synaptic scaling (Turrigiano et al., 1998; Hengen et al., 2013, 2016; Torrado Pacheco et al., 2019, 2021). However, noise exposure did not occlude the effects of high K^+ on Q, and our previous work found no effect of noise exposure on Q (Ngodup et al., 2015; Zhuang et al., 2020; Wong and Xu-Friedman, 2022). Furthermore, in the present experiments, neither the NO donor PAPA-NONOate nor optogenetic stimulation influenced Q, suggesting high K^+ modulates Q through a distinct pathway. Conductive hearing loss appears to cause structural changes in endbulb release sites (Clarkson et al., 2016), and Q has been observed to increase at endbulbs in congenital deafness models (Oleskevich et al., 2004; Mendoza Schulz et al., 2014), suggesting induction of changes in Q may occur during extreme conditions *in vivo*.

References

Arancio O, Lev-Ram V, Tsien RY, Kandel ER, Hawkins RD (1996) Nitric oxide acts as a retrograde messenger during long-term potentiation in cultured hippocampal neurons. J Physiol Paris 90:321–322.

Bellingham MC, Lim R, Walmsley B (1998) Developmental changes in EPSC quantal size and quantal content at a central glutamatergic synapse in rat. J Physiol 511:861–869.

Bender VA, Pugh JR, Jahr CE (2009) Presynaptically expressed long-term potentiation increases multivesicular release at parallel fiber synapses. J Neurosci 29:10974–10978.

Bon CL, Garthwaite J (2003) On the role of nitric oxide in hippocampal long-term potentiation. J Neurosci 23:1941–1948.

Branco T, Staras K (2009) The probability of neurotransmitter release: variability and feedback control at single synapses. Nat Rev Neurosci 10:373–383.

Bredt DS, Snyder SH (1990) Isolation of nitric oxide synthetase, a calmodulin-requiring enzyme. Proc Natl Acad Sci U S A 87:682–685.

Burette A, Petrusz P, Schmidt HH, Weinberg RJ (2001) Immunohistochemical localization of nitric oxide synthase and soluble guanylyl cyclase in the ventral cochlear nucleus of the rat. J Comp Neurol 431:1–10.

Cao XJ, Lin L, Sugden AU, Connors BW, Oertel D (2019) Nitric oxide-mediated plasticity of interconnections between T-stellate cells of the ventral cochlear nucleus generate positive feedback and constitute a central gain control in the auditory system. J Neurosci 39:6095–6107.

Castillo PE (2012) Presynaptic LTP and LTD of excitatory and inhibitory synapses. Cold Spring Harb Perspect Biol 4:a005728.

Chanda S, Xu-Friedman MA (2010) Neuromodulation by GABA converts a relay into a coincidence detector. J Neurophysiol 104:2063–2074.

Chen C, Regehr WG (1997) The mechanism of cAMP-mediated enhancement at a cerebellar synapse. J Neurosci 17:8687–8694.

Clarkson C, Antunes FM, Rubio ME (2016) Conductive hearing loss has long-lasting structural and molecular effects on presynaptic and postsynaptic structures of auditory nerve synapses in the cochlear nucleus. J Neurosci 36:10214–10227.

Coomber B, Kowalkowski VL, Berger JI, Palmer AR, Wallace MN (2015) Modulating central gain in tinnitus: changes in nitric oxide synthase in the ventral cochlear nucleus. Front Neurol 6:53.

Dachtler J, Hardingham NR, Glazewski S, Wright NF, Blain EJ, Fox K (2011) Experience-dependent plasticity acts via GluR1 and a novel neuronal nitric oxide synthase-dependent synaptic mechanism in adult cortex. J Neurosci 31:11220–11230.

Daniel H, Hemart N, Jaillard D, Crepel F (1993) Long-term depression requires nitric oxide and guanosine 3':5' cyclic monophosphate production in rat cerebellar Purkinje cells. Eur J Neurosci 5:1079–1082.

Fourcaudot E, Gambino F, Humeau Y, Casassus G, Shaban H, Poulain B, Lüthi A (2008) cAMP/PKA signaling and RIM1alpha mediate presynaptic LTP in the lateral amygdala. Proc Natl Acad Sci U S A 105:15130–15135.

Gardner SM, Trussell LO, Oertel D (1999) Time course and permeation of synaptic AMPA receptors in cochlear nuclear neurons correlate with input. J Neurosci 19:8721–8729.

Grothe B, Pecka M, McAlpine D (2010) Mechanisms of sound localization in mammals. Physiol Rev 90:983–1012.

Haj-Dahmane S, Béïque JC, Shen RY (2017) GluA2-lacking AMPA receptors and nitric oxide signaling gate spike-timing-dependent potentiation of glutamate synapses in the dorsal raphe nucleus. eNeuro 4:ENEURO.0116-17.2017.

Hengen KB, Lambo ME, Van Hooser SD, Katz DB, Turrigiano GG (2013) Firing rate homeostasis in visual cortex of freely behaving rodents. Neuron 80:335–342.

Hengen KB, Torrado Pacheco A, McGregor JN, Van Hooser SD, Turrigiano GG (2016) Neuronal firing rate homeostasis is inhibited by sleep and promoted by wake. Cell 165:180–191.

Hockley A, Berger JI, Palmer AR, Wallace MN (2020) Nitric oxide increases gain in the ventral cochlear nucleus of guinea pigs with tinnitus. Eur J Neurosci 52:4057–4080.

Huang YY, Kandel ER (1998) Postsynaptic induction and PKA-dependent expression of LTP in the lateral amygdala. Neuron 21:169–178.

Isaacson JS, Walmsley B (1996) Amplitude and time course of spontaneous and evoked excitatory postsynaptic currents in bushy cells of the anteroventral cochlear nucleus. J Neurophysiol 76:1566–1571.

Jacoby S, Sims RE, Hartell NA (2001) Nitric oxide is required for the induction and heterosynaptic spread of long-term potentiation in rat cerebellar slices. J Physiol 535:825–839.

Kopp-Scheinpflug C, Forsythe ID (2021) Nitric oxide signaling in the auditory pathway. Front Neural Circuits 15:759342.

Kronander E, Michalski N, Lebrand C, Hornung JP, Schneggenburger R (2017) An organotypic slice culture to study the formation of calyx of Held synapses in-vitro. PLoS One 12:e0175964.

Kuenzel T (2019) Modulatory influences on time-coding neurons in the ventral cochlear nucleus. Hear Res 384:107824.

Lau C, Zhang JW, McPherson B, Pienkowski M, Wu EX (2015) Long-term, passive exposure to non-traumatic acoustic noise induces neural adaptation in the adult rat medial geniculate body and auditory cortex. Neuroimage 107:1–9.

Lorente de Nó R (1981) The primary acoustic nuclei. New York: Raven.

Malenka RC, Bear MF (2004) LTP and LTD: an embarrassment of riches. Neuron 44:5–21.

Mendoza Schulz A, Jing Z, Sánchez Caro JM, Wetzel F, Dresbach T, Strenzke N, Wichmann C, Moser T (2014) Bassoon-disruption slows vesicle replenishment and induces homeostatic plasticity at a CNS synapse. EMBO J 33:512–527.

Munguia R, Pienkowski M, Eggermont JJ (2013) Spontaneous firing rate changes in cat primary auditory cortex following long-term exposure to non-traumatic noise: tinnitus without hearing loss? Neurosci Lett 546:46–50.

Ngodup T, Goetz JA, McGuire BC, Sun W, Lauer AM, Xu-Friedman MA (2015) Activity-dependent, homeostatic regulation of neurotransmitter release from auditory nerve fibers. Proc Natl Acad Sci U S A 112:6479–6484.

Oleskevich S, Walmsley B (2002) Synaptic transmission in the auditory brainstem of normal and congenitally deaf mice. J Physiol 540:447–455.

Oleskevich S, Youssoufian M, Walmsley B (2004) Presynaptic plasticity at two giant auditory synapses in normal and deaf mice. J Physiol 560:709–719.

Olthof BMJ, Gartside SE, Rees A (2019) Puncta of neuronal nitric oxide synthase (nNOS) mediate NMDA receptor signaling in the auditory midbrain. J Neurosci 39:876–887.

Pienkowski M, Eggermont JJ (2009) Long-term, partially-reversible reorganization of frequency tuning in mature cat primary auditory cortex can be induced by passive exposure to moderate-level sounds. Hear Res 257:24–40.

Pienkowski M, Munguia R, Eggermont JJ (2013) Effects of passive, moderate-level sound exposure on the mature auditory cortex: spectral edges, spectrotemporal density, and real-world noise. Hear Res 296:121–130.

Pliss L, Yang H, Xu-Friedman MA (2009) Context-dependent effects of NMDA receptors on precise timing information at the endbulb of Held in the cochlear nucleus. J Neurophysiol 102:2627–2637.

Qiu DL, Knöpfel T (2007) An NMDA receptor/nitric oxide cascade in presynaptic parallel fiber-Purkinje neuron long-term potentiation. J Neurosci 27:3408–3415.

Regehr WG, Stevens CF (2001) Physiology of synaptic transmission and short-term plasticity. In: Synapses (Cowan WM, SüdhofTC, Stevens CF, eds), pp 135–175. Baltimore: Johns Hopkins UP.

Regehr WG, Carey MR, Best AR (2009) Activity-dependent regulation of synapses by retrograde messengers. Neuron 63:154–170.

Rüttiger L, Zimmermann U, Knipper M (2017) Biomarkers for hearing dysfunction: facts and outlook. ORL J Otorhinolaryngol Relat Spec 79:93–111.

Ryugo DK, Fekete DM (1982) Morphology of primary axosomatic endings in the anteroventral cochlear nucleus of the cat: a study of the endbulbs of Held. J Comp Neurol 210:239–257.

Ryugo DK, Sento S (1991) Synaptic connections of the auditory nerve in cats: relationship between endbulbs of Held and spherical bushy cells. J Comp Neurol 305:35–48.

Sheppard AM, Chen GD, Manohar S, Ding D, Hu BH, Sun W, Zhao J, Salvi R (2017) Prolonged low-level noise-induced plasticity in the peripheral and central auditory system of rats. Neuroscience 359:159–171.

Shore SE, Wu C (2019) Mechanisms of noise-induced tinnitus: insights from cellular studies. Neuron 103:8–20.

Steinert JR, Kopp-Scheinpflug C, Baker C, Challiss RA, Mistry R, Haustein MD, Griffin SJ, Tong H, Graham BP, Forsythe ID (2008) Nitric oxide is a volume transmitter regulating postsynaptic excitability at a glutamatergic synapse. Neuron 60:642–656.

Torrado Pacheco A, Tilden EI, Grutzner SM, Lane BJ, Wu Y, Hengen KB, Gjorgjieva J, Turrigiano GG (2019) Rapid and active stabilization of visual cortical firing rates across light-dark transitions. Proc Natl Acad Sci U S A 116:18068–18077.

Torrado Pacheco A, Bottorff J, Gao Y, Turrigiano GG (2021) Sleep promotes downward firing rate homeostasis. Neuron 109:530–544.e6.

Turrigiano GG (2008) The self-tuning neuron: synaptic scaling of excitatory synapses. Cell 135:422–435.

Turrigiano GG, Leslie KR, Desai NS, Rutherford LC, Nelson SB (1998) Activity-dependent scaling of quantal amplitude in neocortical neurons. Nature 391:892–896.

Tzounopoulos T, Kim Y, Oertel D, Trussell LO (2004) Cell-specific, spike timing-dependent plasticities in the dorsal cochlear nucleus. Nat Neurosci 7:719–725.

Vitureira N, Letellier M, Goda Y (2012) Homeostatic synaptic plasticity: from single synapses to neural circuits. Curr Opin Neurobiol 22:516–521.

Wang M, Zhang C, Lin S, Wang Y, Seicol BJ, Ariss RW, Xie R (2021) Biased auditory nerve central synaptopathy is associated with age-related hearing loss. J Physiol 599:1833–1854.

Wang YX, Wenthold RJ, Ottersen OP, Petralia RS (1998) Endbulb synapses in the anteroventral cochlear nucleus express a specific subset of AMPA-type glutamate receptor subunits. J Neurosci 18:1148–1160.

Whitton JP, Polley DB (2011) Evaluating the perceptual and pathophysiological consequences of auditory deprivation in early postnatal life: a comparison of basic and clinical studies. J Assoc Res Otolaryngol 12:535–547.

Wong NF, Xu-Friedman MA (2022) Time course of activity-dependent changes in auditory nerve synapses reveals multiple underlying cellular mechanisms. J Neurosci 42:2492–2502.

Yang H, Xu-Friedman MA (2012) Emergence of coordinated plasticity in the cochlear nucleus and cerebellum. J Neurosci 32:7862–7868.

Yang Z, Ding K, Pan L, Deng M, Gan L (2003) Math5 determines the competence state of retinal ganglion cell progenitors. Dev Biol 264:240–254.

Yassin L, Radtke-Schuller S, Asraf H, Grothe B, Hershfinkel M, Forsythe ID, Kopp-Scheinpflug C (2014) Nitric oxide signaling modulates synaptic inhibition in the superior paraolivary nucleus (SPN) via cGMP-dependent suppression of KCC2. Front Neural Circuits 8:65.

Zhuang X, Sun W, Xu-Friedman MA (2017) Changes in properties of auditory nerve synapses following conductive hearing loss. J Neurosci 37:323–332.

Zhuang X, Wong NF, Sun W, Xu-Friedman MA (2020) Mechanisms and functional consequences of presynaptic homeostatic plasticity at auditory nerve synapses. J Neurosci 40:6896–6909.

Zimmer A, Zimmer AM, Hohmann AG, Herkenham M, Bonner TI (1999) Increased mortality, hypoactivity, and hypoalgesia in cannabinoid CB1 receptor knockout mice. Proc Natl Acad Sci U S A 96:5780–5785.